Journal Pre-proofs

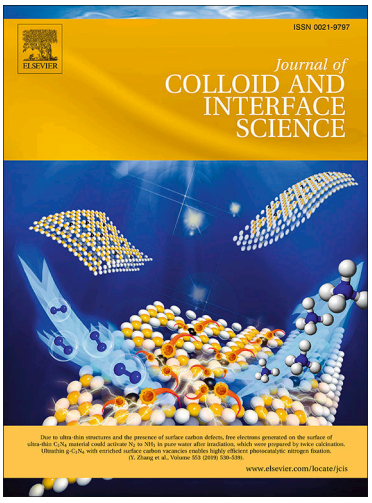

Facile Preparation of $CoMoO_4$ Nanorods at Macroporous Carbon Hybrid Electrocatalyst for Non-enzymatic Glucose Detection

Tianjiao Meng, Huixian Jia, Huimin Ye, Tao Zeng, Xinjian Yang, Huan Wang, Yufan Zhang

PII: S0021-9797(19)31232-9
DOI: https://doi.org/10.1016/j.jcis.2019.10.054
Reference: YJCIS 25548

To appear in: *Journal of Colloid and Interface Science*

Received Date: 13 August 2019
Revised Date: 12 October 2019
Accepted Date: 14 October 2019

Please cite this article as: T. Meng, H. Jia, H. Ye, T. Zeng, X. Yang, H. Wang, Y. Zhang, Facile Preparation of $CoMoO_4$ Nanorods at Macroporous Carbon Hybrid Electrocatalyst for Non-enzymatic Glucose Detection, *Journal of Colloid and Interface Science* (2019), doi: https://doi.org/10.1016/j.jcis.2019.10.054

Facile Preparation of $CoMoO_4$ Nanorods at Macroporous Carbon Hybrid Electrocatalyst for Non-enzymatic Glucose Detection

Tianjiao Meng[a], Huixian Jia[a], Huimin Ye[a], Tao Zeng[b], Xinjian Yang[a], Huan Wang[a*] and Yufan Zhang[a*]

a Key Laboratory of Medicinal Chemistry and Molecular Diagnosis of Ministry of Education, Key Laboratory of Analytical Science and Technology of Hebei Province, College of Chemistry and Environmental Science, Hebei University, Baoding, Hebei 071002, China

b College of Environment, Zhejiang University of Technology, Hangzhou, Zhejiang 310014, China

Abstract

Glucose is a popular biosensor target due to its closely with diabetes or hypoglycemia in blood. Designing efficiency electrocatalysts for the determination of glucose is vital to develop glucose detection devices. $CoMoO_4$, as a kind of bimetallic oxide material, exhibits unique electrochemical properties. 3D macroporous carbon (MPC) has large specific surface area and excellent electrical conductivity, providing an effective support for loading other nano-entities to form novel composite with good synergetic effects. Herein, nanorod-like $CoMoO_4$ anchored onto MPC support was

*Corresponding author: Tel.: +86 03125079403; Fax: +86 03125079403.
E-mail address: zyf@hbu.edu.cn (Y.F. Zhang).

synthesized for the development of a promising electrochemical sensing platform for glucose. Attributing to the synergic effects between the good electrocatalytic performance of $CoMoO_4$ nanorods and the extraordinary electrical conductivity of 3D layered MPC, the novel $CoMoO_4$/MPC composites non-enzymatic sensor shows excellent electrocatalytic performance for oxidation of glucose. Under the optimum conditions, the proposed $CoMoO_4$/MPC hybrids provided a reliable linear range of 5×10^{-7} to 1.08×10^{-4} M with a low limit of detection (0.13 μM) for the detection of glucose. Meanwhile, the $CoMoO_4$/MPC sensing platform shows fast response time of 1.76 s, good stability and selectivity for detecting glucose. Moreover, this non-enzymatic sensor also has been successfully applied to measure glucose level in human blood samples. Therefore, the developed sensor holds a new promise for the construction of facile and sensitive non-enzymatic glucose analytical platform.

Keywords: $CoMoO_4$ nanorods; Macroporous carbon; Electrochemical sensors; Non-enzymatic; Glucose

1. Introduction

Diabetes mellitus as a global chronic disease is of great importance to physiology. The disease originates from insulin deficiency, which is characterized by elevated levels of blood glucose [1, 2]. In addition, diabetes can lead to a range of secondary complications like heart disease, blindness, or kidney failure. Thus, it is vital for the sensitive monitor the content of glucose in human blood. Up to now, various sensing technologies have been established to determine accurate glucose, such as high performance liquid chromatography [3-5], spectrophotometers, colorimetric [6-8], fluorescent techniques [9, 10], and chemiluminescence [11, 12]. Besides, electroanalytical technique is playing a vital role in human blood glucose detection owing to its favorable performance, simple operation, high sensitivity and low cost [13-23].

Enzyme-based electrochemical biosensors have drawn extensive concern, thanks to their extraordinary properties for detecting glucose in human blood matrix. However, enzyme-based biosensors still confronted with the drawback of their poor stability [24, 25]. As well, it impedes the development of enzyme-based biosensors due to the time-consuming and expensive for the synthesis and purification processes of enzymes. Though Noble metal catalysts exhibit considerable catalytic activities toward glucose oxidation, they were limited in human blood glucose detection due to their scarcity and high cost.

Recently, transition metal oxide materials as electrocatalysts have drawn increasing attention due to their superior catalytic and excellent stability [26, 27]. In

addition, bimetallic oxide materials have been widely applied in many fields, such as optical magnetic materials [28], fibers [29], high-performance supercapacitors [30, 31] and sensors, because of its low cost, good biocompatibility, low biological toxicity and excellent electrochemical performances [32, 33]. $CoMoO_4$, as a common bimetallic oxide material, are taking more and more attention in the electrocatalysis field, due to its variable valence states of metal cobalt and molybdenum.

3D macroporous carbon (MPC) has continuously interconnected macroporous structures with high specific surface area, extraordinary electrical conductivity, and good stability [34-37]. In addition, MPC is of great interest for many potential applications because of their 3D porous structure is ideal to serve as the scaffold for the fabrication of hybrid electrode materials.

Herein, we described a facile and cost-effective strategy for the growth of $CoMoO_4$ nanorods loaded on 3D MPC matrix. The novel $CoMoO_4$/MPC composites were investigated as an effective electrocatalyst for the oxidation of glucose. Compared with the pure $CoMoO_4$ nanorods, the $CoMoO_4$/MPC hybrids exhibit excellent electrochemical performances for the detection of glucose, including high sensitivity, wide linear detection range and long-term stability. Moreover, the proposed glucose sensor could produce steady-state signals within 2 s. These superior performances are attributed to the unique catalytic properties of $CoMoO_4$ nanorods and the excellent electrical conductivity of MPC. The as-prepared $CoMoO_4$/MPC composites will provide a promising way for further development of electrochemical sensor for sensitive and fast glucose detection.

2. Experimental

2.1. *Chemical reagents*

Glucose, NaOH, $Co(NO_3)_2 \cdot 6H_2O$, Na_2MoO_4, glycine, L(+)-Cysteine, ascorbic acid, dopamine hydrochloride, L-Phenylalanine, D-Tyrosine, L(+)-Arginine, L-Tyrosine were all provided by Shanghai Macklin Biochemical Co., Ltd. All other reagents used in the synthesis of $CoMoO_4$/MPC composites were of analytical grade and used without further purification.

2.2. *Instrumentation*

Electrochemical impedance spectroscopy (EIS) and cyclic voltammetry (CV) were operated on Autolab Electrochemistry Workstation with a potentiostat PGSTAT 302N (Metrohm, Switzerland). Amperometric i-t electrochemical method was carried out with CHI 660D electrochemical analyzer (Shanghai Chenhua Instrument, Co., China). Scanning electron microscopy (SEM, PhilipsXL-30 ESEM, operating at 3.0 kV) and transmission electron microscopy (TEM, JEM-2100F) were used for morphologies analysis of the as-prepared materials. Fourier transform infrared (FT-IR) spectroscopy of the materials was obtained in a Nicolet Magna 560 FT-IR spectrometer. The structure of materials were investigated by X-Ray diffraction (XRD) using X-ray D/max-2200vpc (Rigaku Corporation, Japan) instrument (k=0.15406 nm). N_2 adsorption-desorption isotherms were carried out by Autosorb-iQASIQ (Quantachrome, USA). The elemental composition of the products was examined using X-ray photoelectron spectroscopy (XPS), which was performed on a thermo ESCA LAB spectrometer.

Raman spectroscopy measurements were further applied to confirm the crystal structures by a Horiba JY-HR800 micro-Raman, Japan. Thermogravimetric analysis (TGA) was investigated by Perkin Elmer Diamond TG analyzer.

2.3. *Synthesis of $CoMoO_4$/MPC composites*

The MPC was synthesized with a standard protocol [38, 39]. For $CoMoO_4$/MPC composites, 0.36 g $Co(NO_3)_2 \cdot 6H_2O$ and 0.26 g Na_2MoO_4 were dispersed in 25 mL distilled water with continuous stirring. Later, 50 mg MPC was added into the mixture solution under the magnetic stirring. Subsequently, the mixture was transferred to a Teflon (100 mL) liner and kept at 150 ^oC for 6 h in drying oven. Finally, the products were centrifuged, and thoroughly washed with deionized water, and then dried at 60 ^oC in drying oven. A graphic of the preparation of $CoMoO_4$/MPC hybrids is shown in Scheme 1.

For the optimization of the ratio of $CoMoO_4$ and MPC, the different content of MPC (70, 50 and 38.9 mg) were added into the mixture, respectively. The $CoMoO_4$/MPC hybrids are named as $CoMoO_4$/MPC-*1*, $CoMoO_4$/MPC-*2* and $CoMoO_4$/MPC-*3*, where *1*, *2* and *3* represent of MPC (70, 50, and 38.9 mg) in the synthesis procedure, respectively.

2.4. *Fabrication of the modified electrodes*

The electrochemical system consisted of a conventional three-electrode system, working electrode: the glassy carbon electrode (GCE) was polished with 50 nm alumina power, followed cleaned by ultrasonic thoroughly; reference electrode: an Ag/AgCl electrode; counter electrodes: a platinum electrode. Electrocatalysts (2 mg) were

dissolved in Nafion (1 mL) solution by ultrasonic dispersion. After that, 5 μL of the resulting suspension were dropped onto a pretreated GCE surface, then the modified electrodes were dried at 25 ^{o}C.

Scheme 1

3. Results and discussion

3.1. Characterization of $CoMoO_4$ microrods and $CoMoO_4$/MPC-*2* composites.

In this work, the MPC can act as a structure-directing template in influencing the crystal growth of $CoMoO_4$ crystallites. Since carboxylic groups and defect sites are present on the MPC surface, it is expected that they might anchor the active metal central cations. The crystals can generate grow on the surface or in the channels of MPC. The morphologies and structures of as-prepared samples were characterized using SEM and TEM images. In Fig.1A and B, pure microrods-like $CoMoO_4$ materials with the length of about 4 μm were presented. Fig.1C shows the TEM image of $CoMoO_4$ microrods, confirming that $CoMoO_4$ nanorods have diameters of about 0.23 μm. The high-resolution TEM image displays the interplanar spacing of 0.33 nm (Fig.1D), corresponding to the (-131) planes of monoclinic $CoMoO_4$. Fig.1E exhibits the SEM image of MPC, illustrating the interconnected macroporous nanostructure of MPC matrix. Interestingly, as can be seen from the SEM image of $CoMoO_4$/MPC-*2* composite, the sizes of $CoMoO_4$ microrods decrease obviously (less than 1μm). The reason may be due to the MPC skeleton make a restriction effect on the growth of $CoMoO_4$ crystallites.

Fig.1

The X-ray diffraction (XRD) results of $CoMoO_4$ microrods, pure MPC matrix, and $CoMoO_4$/MPC-*2* composite are shown in Fig.2A. The patterns of $CoMoO_4$ microrods (curve a) are corresponded with the standard patterns of $CoMoO_4$ (JCPDS 21-0868) [40]. From curve b, a visible reflection of MPC is detected, which is consistent with the characteristic peak of carbon-based materials. The XRD patterns of $CoMoO_4$/MPC-*2* materials (curve c) are in agreement with the simulated patterns of $CoMoO_4$ microrods, thus demonstrating that incorporation of MPC does not disrupt or destroy the crystal structure of $CoMoO_4$.

The as-prepared samples are characterized using FT-IR spectra (Fig.2B). $CoMoO_4$ microrods (curve a) show two characteristics peaks at 955 cm^{-1} and 737 cm^{-1}, corresponding to the vibrational modes of distorted MoO_4 and Mo-O[32]. The vibration band at 433 cm^{-1} attributed to the Co and Mo building blocks of $CoMoO_4$ [41]. The spectra of $CoMoO_4$/MPC-*2* (curve c) largely resembles that of $CoMoO_4$ microrods, also confirming that the successfully prepared of $CoMoO_4$/MPC-*2* hybrids.

Raman spectra were also employed to examine the characterization of the samples (Fig.2C). The characteristics of bands at 931 cm^{-1}, 872 cm^{-1} and 811 cm^{-1} can be observed (curve a), corresponding to the Mo-O-Co stretching vibrations of $CoMoO_4$ microrods. The band located at 361 cm^{-1} can be corresponded to the MoO_4 vibrations. The defined Raman spectra characteristics of D band (1346 cm^{-1}) and G band (1588 cm^{-1}) of MPC support provide the evidence of defects of carbon structure (curve b). The main characteristics bands of $CoMoO_4$ and MPC are observed from

$CoMoO_4$/MPC-*2* (curve c), confirming the successful synthesis of the $CoMoO_4$/MPC-*2* composite. In addition, the G band of $CoMoO_4$/MPC-*2* was down shift than that of MPC matrix, illustrating the presents of strong interaction between $CoMoO_4$ and MPC support [31]. The intensity ratio of MPC (I_D/I_G =0.968) is lower than that of $CoMoO_4$/MPC (I_D/I_G =0.993), which indicates the more defect sites in $CoMoO_4$/MPC-*2* hybrids.

Nitrogen adsorption measurements were used to verify the porous feature of the samples (Fig.2D). The MPC support has the characteristic of large pores (type IV isotherm) with a Brunauer-Emmett-Teller (BET) surface area of 388.5 $m^2 g^{-1}$ (curve b). The BET surface areas of $CoMoO_4$ microrods (curve a) and $CoMoO_4$/MPC-*2* composites (curve c) are 22.24 $m^2 g^{-1}$ and 105.0 $m^2 g^{-1}$, respectively; one can conclude that loading of $CoMoO_4$ microrods on MPC support can enhance the nitrogen uptake by showing BET surface areas.

Fig.2

The typical TGA curves of $CoMoO_4$ microrods and $CoMoO_4$/MPC-*x* composites are shown in Fig.S1. For $CoMoO_4$ microrods (A), an obvious weight loss at 100-190 ^oC is due to the removal of physisorbed H_2O. The weight loss at 190-360 ^oC is observed, which is mainly ascribed to the decomposition of the reactants. An approximate platform is observed after 360 ^oC, indicating the formation of stable products. As for $CoMoO_4$/MPC-*x* composites (B-D), the substantial weight loss after 450 ^oC accompanies the combustion of MPC supports. The mass fraction of $CoMoO_4$ is about

80.86%, 85.16% and 89.29% in the CoMoO4/MPC-*1*, CoMoO4/MPC-*2* and CoMoO4/MPC-*3* nanocomposites, respectively.

Fig.3

The elements compositions of $CoMoO_4$/MPC-*2* hybrids were further performed with XPS spectra. As demonstrated in Fig.3A, wide XPS survey spectrum confirms the presence of C, O, Mo and Co elements in the $CoMoO_4$/MPC-*2* hybrids. The results of XPS survey spectra also shows the atomic percentages analyzed of 49.76% (C), 39.28% (O), 7.43% (Mo) and 3.61% (Co), respectively. In particular, the prominent peak at 288.5 eV is attributed to C 1s (Fig.3B). In Fig.3C, the major peaks located at 530.2 and 532.6 eV are characteristics of metal-oxygen bonds and defect oxygen peak, respectively [42]. Fig.3D shows two prominent peaks at 232 and 235.2 eV, which is attributed to Mo $3d_{5/2}$ and Mo $3d_{3/2}$, respectively [43, 44]. Fig.3E displays Co 2p XPS survey spectrum with two prominent peaks at 780.8 and 797 eV, corresponding to Co $2p_{3/2}$ and Co $2p_{1/2}$ [45].

3.2. *Electrochemical behavior of glucose and its detection*

Electrochemical impedance spectroscopy (EIS) experiments were conducted to verify the electron transfer kinetics of the modified electrode surfaces. As seen in Fig.4, the EIS curves of the bare GCE (a), $CoMoO_4$-GCE (b), MPC-GCE (c), and $CoMoO_4$/MPC-*2*-GCE (d) were investigated in 5 mM $Fe[(CN)_6]^{4-/3-}$ containing 0.1 M KCl with a frequency range of 10^{-2}-10^6 Hz. The small well-defined semicircle of the bare GCE was observed (R_{ct} =138 Ω). After being modified with $CoMoO_4$ microrods,

a large semicircle can be observed (R_{ct} =7.51×10^3 Ω). For the $CoMoO_4$/MPC-*2* composites, attributing to the excellent conductivity of MPC, the R_{ct} value decreased to 409 Ω by loading $CoMoO_4$ with MPC support.

Fig.4

Cyclic voltammogram (CV) is an effective method to study the electrocatalytic performance for the oxidation of glucose. Fig.5 exhibits CV curves of bare GCE (A), $CoMoO_4$-GCE (B) and $CoMoO_4$/MPC-*2*-GCE (C) conducted in the presence (red lines) and absence (black lines) glucose (2.0 mM) in 0.1 M NaOH aqueous solution. It exhibits a weak electrocatalytic oxidation current for glucose at bare GCE (Fig.5A). Furthermore, it shows a markedly increased signal for glucose oxidation at $CoMoO_4$-GCE (Fig.5B). The $CoMoO_4$-GCE shows two well-defined redox pairs with potential ranges between 0.15-0.30 V and 0.30-0.40 V, which corresponded to the quasi-reversible redox process of Co^{2+}/Co^{3+} and Mo^{4+}/Mo^{6+}. The enhanced electrocatalytic activity is attributed to multiple valence states of the $CoMoO_4$ with different metal ions. Compared with $CoMoO_4$-GCE, the oxidation response current for glucose was much higher at the $CoMoO_4$/MPC-*2*-GCE (Fig.5C). This is because of the synergistic effect of good conductivity of MPC supports and unique electrocatalytic performance of $CoMoO_4$ microrods. Fig.S3 shows the CV curves of $CoMoO_4$/MPC-1-GCE, $CoMoO_4$/MPC-*2*-GCE and $CoMoO_4$/MPC-*3*-GCE in the presence of glucose. Compared with the $CoMoO_4$/MPC-*1* and $CoMoO_4$/MPC-*3* electrocatalysts, the much higher current densities on $CoMoO_4$/MPC-*2* for electrocatalytic oxidation of glucose,

which can be ascribed to the suitable configurations of $CoMoO_4$ in the $CoMoO_4$/MPC nanohybrids. Thus, $CoMoO_4$/MPC-*2* was selected as an amperometric sensor for glucose.

Fig.5

In order to examine the electrochemical behaviors of glucose on $CoMoO_4$/MPC-*2*-GCE, CV curves of $CoMoO_4$/MPC-*2*-GCE was tested at various scan rates (Fig.6A). The peak currents increase linearly with the increase of the scan rates at 0.55 V (5-100 mV s^{-1}), which indicates that the kinetics of the interfacial Faradic redox reactions and the electrochemical kinetics is a surface-controlled process (Fig.6B). As shown in Fig.S2, $CoMoO_4$/MPC-*2*-GCE exhibits a large double-layer capacitance (C_{dl}) value of 55.24 mF cm^{-2}, which indicated the high exposure of effective active sites of $CoMoO_4$/MPC-*2* composites. Typically, the electrochemically active surface area (ECSA) is estimated by probing the C_{dl}. Besides, the ECSA is proportional to the C_{dl}, which could evaluate the exposed catalytically active sites of the as-prepared materials. The ECSA and roughness (R) were calculated with equation ECSA=$R\times A_{GCE}$ (A_{GCE} =0.0706 cm^2) and $R=C_{sample}/C_{GCE}$. The results show that $CoMoO_4$/MPC composites have a larger value of roughness and ECSA (Table S1).

Fig.6

In order to evaluate the electrocatalytic performance of MPC-GCE, $CoMoO_4$-GCE and $CoMoO_4$/MPC-*2*-GCE toward oxidation of glucose, the current-time method was employed to optimize working potential. For these samples, the results demonstrate that

+0.55 V is the optimal potential for sensitive determination of glucose. As shown in Fig.7, $CoMoO_4$/MPC-*2* hybrids exhibit the largest response current compare with bare MPC and bare $CoMoO_4$. Theoretically, $CoMoO_4$/MPC-*2* hybrids surface could produce more active sites at +0.60 V. However, it could be seen that the $CoMoO_4$/MPC-*2* exhibits worse current values and sensitivity with a working potential at +0.60 V. This fact mainly attributes to the O_2 gas bubbles (oxygen evolution reaction) covering a part of active sites and then weaken the oxidation ability of glucose. Hence, the working potential at +0.55 V was used for further investigations.

Fig.7

Fig.8 shows the typical amperometric i-t curves of different electrocatalysts for the detection of glucose with an applied potential of +0.55 V. For pure MPC (Fig.8A) and $CoMoO_4$ nanorods (Fig.8C), the response current generally reached a steady-state level about 6.03 s and 4.40 s after the glucose addition. The glucose sensor displays a linear range from 7.50×10^{-5} to 7.25×10^{-4} M with a limit of detection of 6.48 μM at MPC (Fig.8B); and a linear range from 1.50×10^{-6} to 5.75×10^{-5} μM with a limit of detection of 0.48 μM at $CoMoO_4$ nanorods (Fig.8D). For $CoMoO_4$/MPC-*2*-GCE, it could be seen that the current reached the steady-state platform is 1.76 s (inset of Fig.8E), indicating the fast response time of this electrochemical sensor. The calibration plots of $CoMoO_4$/MPC-*2*-GCE are linear over a concentration range from 5.0×10^{-7} to 1.08×10^{-4} M of glucose with a low limit of detections of 0.13 μM. These results further illustrate that the 3D MPC as a multifunctional platform for supporting $CoMoO_4$ microrods could

show more active sites to form novel hybrid nanomaterials with synergetic effects. The detection parameters are comparable with the sensors reported by other groups (Table S2). In addition, the repeatability has been measured with same electrode (n=10). As shown in Fig.S4, the i-t plots display similar response current when adding glucose into supporting solution (5 μM). An acceptable RSD (4.65%) was obtained, which indicate that this method exhibits a good repeatability. Furthermore, the response current of 5 μM glucose remained at 97.8% of the original value by storing $CoMoO_4$/MPC-*2* GCE at 4 ^oC for 2 weeks, demonstrating the electrochemical sensor has a long-term stability.

Fig.8

To explore the selectivity of the $CoMoO_4$/MPC-*2*-GCE, the possible interferences were studied in the presence of 0.5 μM of various biomolecules (Fig.9). Obviously, the i-t plots display an obvious current rising when glucose was injected into supporting solution (5 μM). Later, various interfering compounds (0.5 μM) were added into the supporting solution. All these results exhibit the excellent anti-interference ability and selectivity of $CoMoO_4$/MPC-*2*-GCE toward the analogous biomolecules.

Fig.9

To evaluate the recovery of the proposed assay strategy for the detection of glucose in human serum samples, various concentrations of glucose were addition into serum. Specifically, the recoveries were obtained by adding glucose standard solution with five repetitions. As exhibited in Table S3, the recoveries and RSD were acceptable. The

results indicate that this method can be used in the determination of glucose in real biological samples with good reliability and veracity.

4. Conclusions

In conclusion, the $CoMoO_4$ microrods supported on MPC were successfully designed and synthesized by a facile hydrothermal method. The 3D MPC as a multifunctional platform for supporting $CoMoO_4$ microrods could show more active sites to form novel hybrid nanomaterials with synergetic effects. The characterization and electrochemical experiments has been systematically studied. The results indicated that the $CoMoO_4$/MPC-*2* hybrids exhibit promising catalytic performance for the oxidation of glucose, which is superior to the individual counterparts. Under the optimum conditions, the proposed $CoMoO_4$/MPC-*2* hybrids provided a reliable linear range of 5×10^{-7} to 1.08×10^{-4} M with a low limit of detection (0.13 μM) for the detection of glucose. Meanwhile, the $CoMoO_4$/MPC-*2* sensing platform shows fast response time of 1.76 s, good stability and selectivity for detecting glucose. Moreover, this non-enzymatic sensor also has been successfully applied to measure glucose level in human blood samples. Therefore, the successful fabrication of $CoMoO_4$/MPC-*2* composites not only hold great promise for the design of non-enzymatic electrochemical sensors for glucose detection, but also provide a new strategy for synthesizing highly active and stable transition metal-based materials.

Acknowledgements

The authors gratefully acknowledge the support from the Priority Strategy Project of Key Laboratory of Medicinal Chemistry and Molecular Diagnosis of Ministry of Education (ts2019003), the Natural Science Foundation of Hebei Province (No. B2019201407 and No. B2018201221) and the Advanced Talents Incubation Program of the Hebei University (No.801260201026 and No. 801260201023).

References

[1] B.P. Kovatchev, Metrics for glycaemic control-from HbA 1c to continuous glucose monitoring, Nat. Rev. Endocrinol. 13 (2017) 425–436.

[2] D. Yang, S. Afroosheh, J.O. Lee, H. Cho, S. Kumar, R.H. Siddique, et al., Glucose Sensing Using Surface-Enhanced Raman-Mode Constraining, Anal. Chem. 90 (2018) 14269–14278.

[3] Y. Li, J. Wang, N. Sun, C.-h. Deng, Glucose-6-Phosphate-Functionalized Magnetic Microsphere as Novel Hydrophilic Probe for Specific Capture of N-Linked Glycopeptides, Anal. Chem. 89 (2017) 11151–11158.

[4] S. Bae, S.Y. Kim, M.H. Do, C.H. Lee, Y.J. Song, 1,2,3,4,6-Penta-O-galloyl-ß-D-glucose, a bioactive compound in Elaeocarpus sylvestris extract, inhibits varicella-zoster virus replication, Antiviral Res. 144 (2017) 266–272.

[5] L. Servillo, N. D'Onofrio, R. Casale, D. Cautela, A. Giovane, D. Castaldo, et al., Ergothioneine products derived by superoxide oxidation in endothelial cells exposed to high-glucose, Free Radic. Biol. Med., 108 (2017) 8–18.

[6] F. Qiao, Q. Qi, Z. Wang, K. Xu, S. Ai, MnSe-loaded g-C_3N_4 nanocomposite with synergistic peroxidase-like catalysis: Synthesis and application toward colorimetric biosensing of H_2O_2 and glucose, Sens. Actuators B. 229 (2016) 379–386.

[7] W. Nan, Z. Han, F. Hai, S. Ai, Copper nanoparticles modified graphitic carbon nitride nanosheet as peroxidase mimetic for glucose detection, RSC Adv. 5 (2015) 91302–91307.

[8] L. Zhang, X. Hai, C. Xia, X.W. Chen, J.H. Wang, Growth of CuO nanoneedles on

graphene quantum dots as peroxidase mimics for sensitive colorimetric detection of hydrogen peroxide and glucose, Sens. Actuators B. 248 (2017) 374–384.

[9] J.-W. Liu, Y. Luo, Y.-M. Wang, L.-Y. Duan, J.-H. Jiang, R.-Q. Yu, Graphitic Carbon Nitride Nanosheets-Based Ratiometric Fluorescent Probe for Highly Sensitive Detection of H_2O_2 and Glucose, ACS Appl. Mater. Interfaces 8 (2016) 33439–33445.

[10] L. Liu, M. Wang, C. Wang, In-situ synthesis of graphitic carbon nitride/iron oxide-copper composites and their application in the electrochemical detection of glucose, Electrochim. Acta, 265 (2018) 275–283.

[11] N. Georgelis, K. Fencil, M.C. Richael, Validation of a rapid and sensitive HPLC/MS method for measuring sucrose, fructose and glucose in plant tissues, Food Chem. 262 (2018) 191–198.

[12] Q.T. Xue, D.Z. Yi, W.J. Zhong, M.W. Dong, Z.H. Cheng, F.L. Yuan, Fe_3O_4 and metal–organic framework MIL-101 (Fe) composites catalyze luminol chemiluminescence for sensitively sensing hydrogen peroxide and glucose, Talanta, 179 (2018) 43–50.

[13] T. Liu, M. Li, D. Peng, Y. Zhang, L. Guo, Design and facile synthesis of mesoporous cobalt nitride nanosheets modified by pyrolytic carbon for the nonenzymatic glucose detection, Sens. Actuators B. 255 (2018) 1983–1994.

[14] L. Wang, T. Meng, L. Liang, J. Sun, S. Wu, H. Wang, et al., Fabrication of amine-functionalized metal-organic frameworks with embedded palladium nanoparticles for highly sensitive electrochemical detection of telomerase activity, Sens. Actuators, B 278 (2019) 133–139.

[15]M. Li, P. Dong, Y. Zhang, Facile design and synthesis of ultrafine FeCo nanocrystallines coupled with porous carbon nanosheets as high efficiency non-enzymatic glucose sensor, J. Alloy. Compd. 810 (2019) 151927.

[16] L. Wang, T. Meng, G. Yu, S. Wu, J. Sun, H. Jia, et al., A label-free electrochemical biosensor for ultra-sensitively detecting telomerase activity based on the enhanced catalytic currents of acetaminophen catalyzed by Au nanorods, Biosens. Bioelectron. 124-125 (2019) 53–58.

[17] F. Li, R. Li, Y. Feng, T. Gong, M. Zhang, L. Wang, et al., Facile synthesis of Au-embedded porous carbon from metal-organic frameworks and for sensitive detection of acetaminophen in pharmaceutical products, Mater. Sci. Eng. C 95 (2019) 78–85.

[18] L. Wang, T. Meng, H. Jia, Y. Feng, T. Gong, H. Wang, et al., Electrochemical study of hydrazine oxidation by leaf-shaped copper oxide loaded on highly ordered mesoporous carbon composite, J. Colloid Interface Sci. 549 (2019) 98–104.

[19] X. Bo, M. Zhou, L. Guo, Electrochemical sensors and biosensors based on less aggregated graphene, Biosens. Bioelectron. 89 (2017) 167–186.

[20] A. Salah, M. Hassan, J. Liu, M. Li, X. Bo, J.C. Ndamanisha, et al., Pt nanoparticles supported on nitrogen-doped porous graphene for sensitive detection of Tadalafil, J. Colloid Interface Sci. 512 (2018) 379–388.

[21] L. Wang, T. Meng, J. Sun, S. Wu, M. Zhang, H. Wang, et al., Development of Pd/Polyoxometalate/nitrogen-doping hollow carbon spheres tricomponent nanohybrids: A selective electrochemical sensor for acetaminophen, Anal. Chim. Acta 1047 (2019) 28–35.

[22] M. Nosuhi, A. Nezamzadeh-Ejhieh, Comprehensive study on the electrocatalytic effect of copper-doped nano-clinoptilolite towards amoxicillin at the modified carbon paste electrode-solution interface, J. Colloid Interface Sci. 497 (2017) 66–72.

[23] T. Meng, L. Wang, H. Jia, T. Gong, Y. Feng, R. Li, et al., Facile synthesis of platinum-embedded zirconia/porous carbons tri-component nanohybrids from metal-organic framework and their application for ultra-sensitively detection of methyl parathion, J. Colloid Interface Sci. 536 (2019) 424–430.

[24] W. Yin, J. Yu, F. Lv, L. Yan, L.R. Zheng, Z. Gu, et al., Functionalized Nano-MoS_2 with Peroxidase Catalytic and Near-Infrared Photothermal Activities for Safe and Synergetic Wound Antibacterial Applications, ACS Nano. 10 (2016) 11000–11011.

[25] L. Jin, Z. Meng, Y. Zhang, S. Cai, Z. Zhang, C. Li, et al., Ultrasmall Pt Nanoclusters as Robust Peroxidase Mimics for Colorimetric Detection of Glucose in Human Serum, ACS Appl. Mater. Interfaces 9 (2017) 10027–10033.

[26] D. Chen, C. Chen, Z.M. Baiyee, Z. Shao, F. Ciucci, Nonstoichiometric Oxides as Low-Cost and Highly-Efficient Oxygen Reduction/Evolution Catalysts for Low-Temperature Electrochemical Devices, Chem. Rev. 115 (2015) 9869–9921.

[27] M. Li, M. Lu, J. Yang, J. Xiao, L. Han, Y. Zhang, et al., Facile design of ultrafine $CuFe_2O_4$ nanocrystallines coupled porous carbon nanowires: Highly effective electrocatalysts for hydrogen peroxide reduction and the oxygen evolution reaction, J. Alloy. Compd. 809 (2019) 151766.

[28] T. Zeng, S. Li, J. Hua, Z. He, X. Zhang, H. Feng, et al., Synergistically enhancing Fenton-like degradation of organics by in situ transformation from Fe_3O_4 microspheres

to mesoporous Fe, N-dual doped carbon, Sci Total Environ 645 (2018) 550–559.

[29] T. Zeng, M. Yu, H. Zhang, Z. He, J. Chen, S. Song, Fe/Fe_3C@N-doped porous carbon hybrids derived from nano-scale MOFs: robust and enhanced heterogeneous catalyst for peroxymonosulfate activation, Catal. Sci. Technol. 7 (2017) 396–404.

[30] M. Li, Y. Liu, L. Han, J. Xiao, X. Zeng, Y. Zhang, et al., A novel strategy for realizing high nitrogen doping in Fe_3C-embedded nitrogen and phosphorus-co-doped porous carbon nanowires: efficient oxygen reduction reaction catalysis in acidic electrolytes, J. Mater. Chem. A 7 (2019) 17923–17936.

[31] L. Wang, T. Meng, C. Chen, Y. Fan, Q. Zhang, H. Wang, et al., Facile synthesis of ZnCo-ZIFs-derived $Zn_xCo_{3-x}O_4$ hollow polyhedron for efficient oxygen evolution reduction, J. Colloid Interface Sci. 532 (2018) 650–656.

[32] M. Li, J. Yang, M. Lu, Y. Zhang, X. Bo, Facile design of ultrafine Co_7Fe_3 nanoparticles coupled with nitrogen-doped porous carbon nanosheets for non-enzymatic glucose detection, J. Colloid Interface Sci. 555 (2019) 449–459.

[33] Y. Xinzhi, L. Bingan, X. Zhi, Super long-life supercapacitors based on the construction of nanohoneycomb-like strongly coupled CoMoO(4)-3D graphene hybrid electrodes, Adv. Mater. 26 (2014) 1044–1051.

[34] Q. Teng, Y. Chen, X. Sun, Y. Wang, F. Li, L. Wang, et al., Formation of Fe_2O_3 microboxes/ macroporous carbon hybrids from Prussian blue template for electrochemical applications, J. Alloy. Compd. 739 (2018) 425–430.

[35] L.M. Jin, F. He, W.L. Cai, J.X. Huang, B.H. Liu, Z.P. Li, Preparation, characterization and application of modified macroporous carbon with Co N site for

long-life lithium-sulfur battery, J. Power Sources 328 (2016) 536–542.

[36] Y. Song, X. Lu, Y. Li, Q. Guo, S. Chen, L. Mao, et al., Nitrogen-Doped Carbon Nanotubes Supported by Macroporous Carbon as an Efficient Enzymatic Biosensing Platform for Glucose, Anal. Chem. 88 (2016) 1371–1377.

[37] T. Zhang, M. Liu, Q. Zhang, Y. Wang, X. Kong, L. Wang, et al., Sensitive determination of chlorogenic acid in pharmaceutical products based on the decoration of 3D macroporous carbon with Au nanoparticles via polyoxometalates, Analyst, 142 (2017) 2603–2609.

[38] W. Stöber, A. Fink, E. Bohn, Controlled growth of monodisperse silica spheres in the micron size range, J. Colloid Interface Sci. 26 (1968) 62–69.

[39] S. Jun, S.H. Joo, R. Ryoo, M. Kruk, M. Jaroniec, Z. Liu, et al., Synthesis of New, Nanoporous Carbon with Hexagonally Ordered Mesostructure, J. Am. Chem. Soc. 122 (2000) 10712–10713.

[40] W. Jing, Z. Xiang, Q. Wei, H. Lv, Y. Tian, Z. Tong, et al., 3D self-supported nanopine forest-like Co_3O_4 @$CoMoO_4$ core-shell architectures for high-energy solid state supercapacitors, Nano Energy 19 (2016) 222–233.

[41] G. Kianpour, M. Salavati-Niasari, H. Emadi, Precipitation synthesis and characterization of cobalt molybdates nanostructures, Superlattices Microstruct 58(2013) 120–129.

[42] Y.Z. Su, K. Xiao, N. Li, Z.Q. Liu, S.Z. Qiao, Amorphous $Ni(OH)_2$@three-dimensional Ni core-shell nanostructures for high capacitance pseudocapacitors and asymmetric supercapacitors, J. Mater. Chem. A 2 (2014) 13845–13853.

[43] D. Ghosh, S. Giri, C.K. Das, Synthesis, characterization and electrochemical performance of graphene decorated with 1D $NiMoO_4 \cdot nH_2O$ nanorods, Nanoscale, 5 (2013) 10428–10437.

[44] G. Yuan, $CoMoO_4$ nanoparticles anchored on reduced graphene oxide nanocomposites as anodes for long-life lithium-ion batteries, ACS Appl. Mater. Interfaces 6 (2014) 20414–20422.

[45] Z. Zhang, H. Zhang, X. Zhang, D. Yu, J. Ying, Q. Sun, et al., Facile synthesis of hierarchical $CoMoO_4$@$NiMoO_4$ core–shell nanosheet arrays on nickel foam as an advanced electrode for asymmetric supercapacitors, J. Mater. Chem. A 4 (2016) 18578–18584.

Figure caption

Scheme 1 graphic of the preparation of $CoMoO_4$/MPC hybrids.

Fig.1 SEM images of $CoMoO_4$ nanorods (A and B). TEM image of $CoMoO_4$ nanorods (C). High-resolution TEM image of $CoMoO_4$ nanorods (D). SEM images of pure MPC (E) and $CoMoO_4$/MPC-*2* composites (F).

Fig.2 XRD analysis of $CoMoO_4$ nanorods (a), MPC (b) and $CoMoO_4$/MPC-*2* (c) (A). FT-IR spectra of $CoMoO_4$ nanorods (a), MPC (b) and $CoMoO_4$/MPC (c) (B), Raman Spectra of $CoMoO_4$ nanorods (a), MPC (b) and $CoMoO_4$/MPC-*2* (c) (C), (D) Nitrogen adsorption-desorption isotherms of $CoMoO_4$ nanorods (a), MPC (b) and $CoMoO_4$/MPC-*2* (c) (D).

Fig.3 Wide XPS survey spectra of $CoMoO_4$/MPC-*2* composites (A), High-resolution XPS spectra of C 1s (B), O 1s (C), Mo 3d (D) and Co 2p (E) of $CoMoO_4$/MPC-*2* composites.

Fig.4 Nyquist plots of EIS investigated in 5 mM $Fe[(CN)_6]^{4-/3-}$ containing 0.1 M KCl supporting electrolyte: bare GCE (a), $CoMoO_4$-GCE (b), MPC-GCE (c), and $CoMoO_4$/MPC-*2*-GCE (d).

Fig.5 CV curves of bare GCE (A), $CoMoO_4$-GCE (B) and $CoMoO_4$/MPC-*2*-GCE (C) in absence (black lines) and presence (red lines) of 2.0 mM glucose in 0.1 M NaOH solution; Scan rate: 50 mV s^{-1}.

Fig.6 CV curves of $CoMoO_4$/MPC-*2*-GCE in 0.1 M NaOH solution with 2.0 mM glucose at various scan rates (A). The calibration plots of current versus scan rates at 0.55 V (B).

Fig.7 Amperometric i-t curves of containing glucose (0.01-0.08 mM) at different operating voltages (from +0.45 to +0.60 V): pure MPC (A), $CoMoO_4$ nanorods (C), and $CoMoO_4$/MPC-*2* (E). The corresponding calibration plots of glucose concentration vs. current signals: pure MPC (B), $CoMoO_4$ nanorods (D), $CoMoO_4$/MPC-*2* hybrids (F).

Fig.8 Typical amperometric i-t curve addition continuously with glucose at MPC (A), $CoMoO_4$ nanorods (C), and $CoMoO_4$/MPC-*2* (E); insets: response time of different electrodes for glucose. Corresponding calibration curve plotted between the current signals of different electrodes *vs* the concentration of glucose at MPC (B), $CoMoO_4$ nanorods (D), and $CoMoO_4$/MPC-*2* (F); potential: +0.55 V.

Fig.9 Specificity investigation of $CoMoO_4$/MPC-*2*-GCE to glucose by adding several analogous molecules (10% of glucose solution).

Highlights

1 Nanorod-like $CoMoO_4$ at MPC supports were prepared by a simple method.

2 $CoMoO_4$/MPC hybrids were acted as an effective sensing platform for non-enzymatic glucose detection.

3 The novel $CoMoO_4$/MPC hybrids will hold promise in development of electrode materials.

Graphical abstract

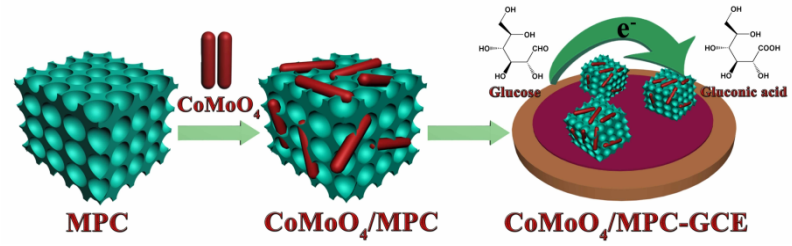

Declaration of interests

☑ The authors declare that they have no known competing financial interests or personal relationships that could have appeared to influence the work reported in this paper.

☐The authors declare the following financial interests/personal relationships which may be considered as potential competing interests: